23-SI-80

CHARACTERIZATION OF INTERNAL BOUNDARY LAYER CAPACITORS

H. D. Park* and D. A. Payne

Department of Ceramic Engineering
and
Materials Research Laboratory

University of Illinois at Urbana-Champaign
Urbana, Illinois 61801

Paper to be presented at the American Ceramic Society

"International Symposium on Grain Boundary Phenomena in Electronic Ceramics"

Tuesday, April 29, 1980, 10:00 a.m.

Submitted for refereeing and publication in

The Proceedings of the International Symposium

ACCEPTED

IN FINAL FORM MAY 12th, 1980

DISCLAIMER

ABSTRACT

Internal boundary layer capacitors were characterized by scanning transmission electron microscopy and by microscale electrical measurements. Data are given for the chemical and physical characteristics of the individual grains and boundaries, and their associated electric and dielectric properties. Segregated internal boundary layers were identified with resistivities of 10^{12}-10^{13} Ω-cm. Bulk apparent dielectric constants were 10,000-60,000. A model is proposed to explain the dielectric behavior in terms of an equivalent n-c-i-c-n representation of ceramic microstructure, which is substantiated by capacitance-voltage analysis.

I. INTRODUCTION

The properties of polycrystalline electrical ceramics are greatly influenced by the electrical and mechanical boundary conditions existing at grain and phase boundaries. Properties may be engineered into polycrystalline systems, which never could be obtained in single crystals alone. They are a function of polycrystallinity. Notable examples include positive temperature coefficient of resistance (PTCR) thermistors and internal boundary layer (IBL) capacitors. The latter are the subject of this characterization study.

Anomalously high apparent dielectric constants ($\bar{K}'$) calculated for IBL capacitors are generally attributed to enhanced space charge polarization processes taking place between semiconducting grains and resistive boundaries. Commercial capacitors are usually manufactured from titanate based materials in the perovskite (ABX_3) family, which are made semiconducting (n-type) by aliovalent chemical substitution, gaseous reduction, or combinations thereof. Resistivity distributions are developed within the microstructure by boundary counterdiffusion (p-type), or by sintering in the presence of a liquid phase which solidifies on cooling into an insulator. Ideally, the former method is characterized by grain to grain contact, with interfacial compensation (c) states; and the latter by grain to grain separation, with an insulating (i) intergranular phase. Commercial units often approximate a hybrid assembly between these two end member conditions.

Several investigations have reported on the preparation and properties of IBL capacitors. In particular, Waku[1-2] reported on the effects of processing conditions, chemical composition, amount and type of dopants, firing practices and resultant dielectric properties. Heywang[3-6], in a pioneering series of papers, developed the concept of potential barriers at grain surfaces. The role of preferentially segregated counterdopants was emphasized. Acceptor states have also been attributed to anion absorption,[7] and increased concentration of

cation (A) vacancies at grain boundaries.[8] Intergranular layers were identified by electron microscopy,[9] decoration techniques,[10] and resistivity probes.[11] p-type intermediate layers have also been suggested.[12] Anomalously high dielectric constants were explained in terms of simplified Maxwell-Wagner theory, where space charge enhancement can be calculated in terms of the limiting case of semiconducting grain thickness to insulating boundary width.[13-14] Electrical measurements of single boundaries in coarse grain material were also attempted by slicing and thinning techniques.[9] In this paper we report on measurements made *in situ* within the microstructure, by using micromanipulators. The IBL capacitors were previously characterized by scanning transmission electron microscopy (STEM) techniques.

II. EXPERIMENTAL METHOD

IBL capacitors were obtained from commercial sources, and were representative of the types of units currently manufactured from $BaTiO_3$ and $SrTiO_3$. They were designated G and J, respectively. In addition, research and development capacitors were prepared in our laboratory from $SrTiO_3$, and were designated I. After bulk capacitance (C) and resistance (R) measurements were made as a function of temperature (T) and voltage (V), apparent dielectric constants ($\bar{K}'$) and resistivities ($\bar{\rho}$) were calculated from geometric consideration. Thin sections were prepared for electron microscopy by diamond wafering and polishing, followed by ion milling.

A Jeol JSEM-200KV electron microscope was used for routine microstructure analysis. Detailed characterization studies were carried out with a Vacuum Generators HP5, which was dedicated to the STEM mode. This particular microscope had a field emission gun, with a typical electron spot size of 5 Å. Point by point chemical analyses were made every 100 Å by energy dispersive analysis of X-rays (EDAX). Microscale electrical measurements were carried

out on polished surfaces, over which a checker-board pattern of electrode pads had been deposited by Pd/Au evaporation through a fine grid network. Contacts were made to electrode pads (25 x 25 μm) by tungsten wire probes (10 μm tips) which were positioned by micromanipulators under a compound optical microscope. The microscope was fitted with a warm stage, so that the temperature dependence of $\bar{K}'$ and $\bar{\rho}$ could be determined for individual grains and boundaries, by selecting appropriate electrode pads.

III. RESULTS AND OBSERVATIONS

1. Microstructure Characterization

Figure 1 illustrates a typical microstructure of a polished and thermally etched surface of a G type IBL capacitor based upon $BaTiO_3$. The grain size ranged between 20-50 μm, with an intergranular phase of anisotropic crystalline morphology. Electron probe microanalysis (EPMA) identified the grains to be $(Ba,Sr)(Ti,Sn)O_3$, and the boundary phase to be titania rich, Ti:Ba>>1. (Si was also found to be preferentially segregated within the boundary phase, with Al only being present in the boundary region.)

A transmission photomicrograph of a replica of a polished and thermally etched surface of a J-1 type IBL capacitor based on $SrTiO_3$ is given in Figure 2. The grain size ranged from 20-60 μm. (The boundary appears unusually wide in this photomicrograph due to thermal grooving). STEM analysis indicated Bi was preferentially concentrated in the boundary region. EPMA data for a polished but unetched surface are given in Figure 3. Integrated intensities as a function of distance illustrate the concentration profile for Bi, which was concentrated in a 300 Å wide boundary region, and extended 100 Å into the grain.

Data for research and development IBL capacitors are given in figures 4 and 5. Figure 4 illustrates the microstructure for a capacitor formed from $SrTiO_3$ powder doped with WO_3, which was fired in a reducing atmosphere. Cu_2O was later diffused in from external surfaces. The capacitor had a $\bar{K}' = 50,000$. The crystalline nature of the counterdoped Cu containing boundary layer is shown by electron diffraction patters. IBL capacitors of a finer microstructure were prepared from prereduced $SrTiO_3$ by liquid phase sintering techniques. The prereduced powder was doped with Bi_2WO_6, calcined in reducing atmospheres, and size reduced. Capacitors formed by liquid phase sintered with $Pb_5Ge_3O_{11}$ were designated I-1, and those sintered with borates I-2. The final grain size was essentially the same as the starting particulate size. Figure 5 illustrates a typical microstructure for an I-1 IBL capacitor. The grain size ranged from 0.5-2 μm, suitable for multilayer capacitors, which have been made. EPMA identified Pb within the boundary phase, the crystalline nature of which was established by selected area electron diffraction.

2. Electrical Measurements

Capacitance measurements were made with a Hewlett-Packard 4270-A automatic bridge and a General Radio 1620-A transformer ratio arm bridge. The a.c. signal was 0.2v at 1 KHz. Figure 6 illustrates the d.c. voltage dependence of $\bar{K}'$ for bulk samples. Dielectric saturation occurred readily with increasing bias for type G IBL capacitors. This is to be expected for ferroelectric materials based upon $BaTiO_3$. Temperature measurements identified a dielectric transition close to room temperature, with a steep Curie-Weiss decay. Type G IBL capacitors were not stable in their properties as temperature and voltage varied, when compared with the behavior of $SrTiO_3$ based capacitors. The great advantage of microstructurally engineering IBL

capacitors from paralectric materials is self evident. In addition, $SrTiO_3$ type I IBL capacitors, which contained an insulating intergranular phase, and which approximated a n-i-n structure, were much more stable in their properties than acceptor compensated type J capacitors. The actual magnitude of $\bar{K}'$ depended on the volume fraction of liquid phase sintering compound used. Measurements for individual boundaries are illustrated in Figure 7. When one considers the actual boundary thickness in unetched samples (0.01-0.1 μm), these measurements do not represent weak field values (e.g., 10^5 v/cm). The capacitance per boundary was approximately 10 pF, with a dissipation factor less than 4%.

Current-voltage measurements were made of the bulk, grain and boundary regions by using a Keithley 610C electrometer. Typical data are given in Figure 8 for a $SrTiO_3$ type J1 IBL capacitor. Calculated resistivities for a suite of samples indicated boundary resistivities to lie between 10^{12} and 10^{13} Ω-cm, with a grain resistivity of approximately 50 Ω-cm. The grains were ohmic in their I-V characteristics whereas the boundaries were nonohmic above 10v. The voltage dependent resistance (VDR) characteristics of the bulk could be modeled on a series network of distributed boundaries. Typical data for the temperature dependence of resistivity for a J-1 type IBL capacitor are given in Figure 9. The insulating grain boundary (GB) material was more temperature dependent than the semiconducting grains (G).

Capacitance-voltage measurements previously indicated the stability of n-i-n type I capacitors, and the voltage dependence of acceptor compensated materials (G and J). Measurements on the latter were made of the bulk and boundary characteristics, and the data analyzed in terms of step (C^{-2} vs. V) or graded (C^{-3} vs. V) junctions. Unambiguous analysis appeared at first, to be not possible. Data given in figure 10 are for various types of

IBL capacitors. The high voltage behavior approximated Schottky type depletion layer characteristics, and the low voltage behavior suggested insulation stabilization. A hybrid model developed to account for these overall characteristics, is discussed in the following section.

IV. Discussion

STEM analysis revealed both the physical and chemical characteristics of the boundary regions. Microscale electrical measurements determined the resistive and dielectric properties of the boundary conditions. Segregated insulation layers and counterdopants were identified. Probe analyses determined the concentration profiles for additives between resistive boundaries and semiconducting grains. This suggests the possible formation of compensated(c) layers between n-type grains and insulating(i) boundaries. A proposed energy band model for acceptor counterdoped IBL capacitors is given in Figure 11.

The diagram is for unbiased thermal equilibrium, and represents a general case between end member n-i-n and n-c-n equivalent representations. It is referred to as the n-c-i-c-n model for IBL phenomena. The potential barrier (V_B) for the junction is similar to a Schottky model, except that an insulating layer is present within part of the depletion region. Figure 11 indicates the insulation layer to extend δ from the center of the boundary region, and the acceptor profile be of width ω. Thus, the intergranular insulation layer is of total width 2δ, and the compensation layer of width $(\omega - \delta)$ in the grain subsurface.

On application of a bias voltage, the barrier is lowered $(V_B - V)$ in the forward sense, and raised $(V_B + V)$ in the reverse case. The total junction capacitance ($\bar{C}$), per unit area, is given by the capacitance of the insulating layer (C_i) and the series connected forward (C_C^F) and reverse

(C_C^R) biased compensation layers, i.e.,

$$\frac{1}{\bar{C}} = \frac{1}{C_i} + \frac{1}{C_C^F} + \frac{1}{C_C^R} \tag{1}$$

which is equivalent to

$$\frac{1}{\bar{C}} = \frac{2\delta}{\varepsilon_o K_i} + \left[\frac{2\,(V_B - V)}{qN_{D+}\varepsilon_o K_c}\right]^{1/2} + \left[\frac{2\,(V_B + V)}{qN_{D+}\varepsilon_o K_c}\right]^{1/2} \tag{2}$$

where, ε_o is the permittivity of free space, K_i and K_c the respective dielectric constants of the insulating and compensation layers, q the electronic charge, and N_{D+} the concentration of uncompensated ionized donors. Two voltage limits therefore exist:

(i) Initially, at V = 0, for a symmetric barrier, $C_C^F = C_C^R$,

$$\frac{1}{\bar{C}} = \frac{2\delta}{\varepsilon_o K_i} + 2\left[\frac{2V_B}{qN_{D+}\varepsilon_o K_c}\right]^{1/2} \tag{3}$$

and

(ii) Finally, at high voltage, $V > V_B$, where reverse biased capacitance dilutes the total series capacitance,

$$\frac{1}{\bar{C}} = \frac{2\delta}{\varepsilon_o K_i} + \left[\frac{2(V_B + V)}{qN_{D+}\varepsilon_o K_c}\right]^{1/2} \tag{4}$$

Examination of equations (2-4) in expanded form, indicates why $(\bar{C})^{-2}$ vs. V data (figure 10) should deviate from linearity, especially at high voltages, due to additional square root terms. Data for single junctions, illustrated in figure 10, have been analysed according to the general n-c-i-c-n model (equation 2). An insulation width of 0.1 μm was taken for 2δ, which was consistant with STEM analysis of unetched surfaces. The $\bar{K}_c'$ value for linear

$SrTiO_3$ was 300. For ferroelectric $BaTiO_3$, a high field value of $\overline{K}'_c(E)$ = 600 was chosen, which is consistent with saturation behavior of (Ba,Sr)(Ti,Sn)O_3. Parameters calculated from intercept and slope data in Figure 11 are summarized below in Table 1.

TABLE 1

Material Parameters for IBL Capacitors

Type	Material	N_{D+} (cm^{-3})	$\overline{K}'_i$	V_B
G	$BaTiO_3$	$1.2 \cdot 10^{18}$	55	0.9
J-1	$SrTiO_3$	$4.0 \cdot 10^{20}$	102	0.8
J-2	$SrTiO_3$	$5.0 \cdot 10^{20}$	39	1.0

These values are in good agreement with cation dopant concentrations (0.3 at %) in air fired type G material, and combined cation and anion concentrations in reduction fired type J material. Calculated dielectric constant values for insulating boundary phase (K_i) are consistent with STEM analysis, which identified a titania rich boundary phase in type G material, and bismuth rich boundaries in type J capacitors. The possibility of bismuth titanate-strontium titanate derived boundary structures in type J-1 IBL capacitors has yet to be established. Values of V_B are consistent with donor levels within the band gap (3-4eV). Thus the n-c-i-c-n model for commercial IBL capacitors appears to be extremely relevant, when one considers all the possible variations from ideal representation.

V. SUMMARY

Internal boundary layer capacitors based upon $BaTiO_3$ and $SrTiO_3$ were characterized by STEM analysis and microscale electrical measurements. The intrinsic properties of individual grains and boundaries were determined, as well as the extrinsic properties of polycrystalline ensembles. Commercial capacitors had a grain size of 20 - 60 μm, and contained a segregated boundary phase. The chemical composition and segregation profile of the boundary regions were determined by EPMA. Data were presented for fine grain multilayer compositions. IBL capacitors containing an insulating boundary phase were extremely stable in their properties, and approximated n-i-n model structures. Capacitors formed by valence counterdoping techniques were voltage sensitive, similar to compensated depletion layer n-c-n model. A hybrid representation of ceramic microstructures was proposed, and properties described in terms of a general n-c-i-c-n model. C^{-2} vs V analyses of single junctions were successful. The boundary resistivities were 10^{12}-10^{13} Ω-cm.

VI. ACKNOWLEDGEMENTS

This work was supported by the Transelco Division of Ferro Corporation and by the Department of Energy. We acknowledge the assistance of P. C. Held, S. M. Park, C. A. T. Suchicital and I. D. Ward.

REFERENCES

1. S. Waku, "Studies on the Boundary Layer Ceramic Capacitor," Rev. Elec. Comm. Lab., 15 (9-10), 689-715 (1967).

2. S. Waku, M. Uchidate and K. Kuichi, "Studies on the (Ba,Sr)TiO_3 Boundary Layer Ceramic Dielectrics," Rev. Elec. Comm. Lab., 18 (9-10), 681-693 (1970).

3. Heywang, W., "Anomalous Semiconductor Effects in $BaTiO_3$," Solid State Phys., 4 877-882 (1960).

4. W. Heywang, "Barium Titanate as a Semiconductor with Blocking Layers," Solid State Electr. 3 (1) 51-58 (1961).

5. W. Heywang, "Resistivity Anomaly in Doped Barium Titanate," J. Am. Ceram. Soc., 47 (10) 484-490 (1964).

6. W. Heywang, "Semiconducting Barium Titanate," J. Mat. Sci., 6 1214-1216 (1971).

7. G. H. Jonker, "Halogen Treatment of Barium Titanate Semiconductor," Mat. Res. Bull., 2 401 (1967).

8. J. Daniels and R. Wernicke, "New Aspects of an Improved PTC Model," Philips Res. Repts. 31 489-504, (1976).

9. H. Rehme, "Elektronenmikroskopischer Nachweis von Sperrschichten in Bariumtitanat-Kaltleiterkeramik," Phy. Stat. Sol., 18 k101 (1966).

10. P. Gerthsen and K. M. Hardtl, "Method for Proof of Inhomogeneity of Conduction at Grain Boundaries," Z. Naturforsch 18a, 423-24 (1963).

11. P. Gerthsen, and B. Hoffmann, "Current-Voltage Characteristics and Capacitance of Single Grain Boundaries in Semiconducting $BaTiO_3$ Ceramics," Sol. Stat. Elec., 16 617 (1973).

12. H. Brauer, "Korngrenzensperrschichten in $BaTiO_3$-Keramik mit hoher effektiver kielektrizitatskonstante," Z. angew. Phys., 29 282 (1970).

13. T. Edahiro and F. Yoshimura, "Experiments on Boundary Layer Dielectrics with Low Temperature Coefficients," Rev. Elec. Comm. Lab., 21 (11-12) 843-853 (1973).

14. D. L. Johnson and R. T. McSweeney, "Correlation of Properties to Microstructure of a Boundary Layer Capacitor," Ceramic Microstructures '76, 598-609, Westview Press (1977).

15. B. R. Gossick, Potential Barriers in Semiconductors, 89-94, Academic Press, N.Y., (1964).

LIST OF FIGURES

Fig 1

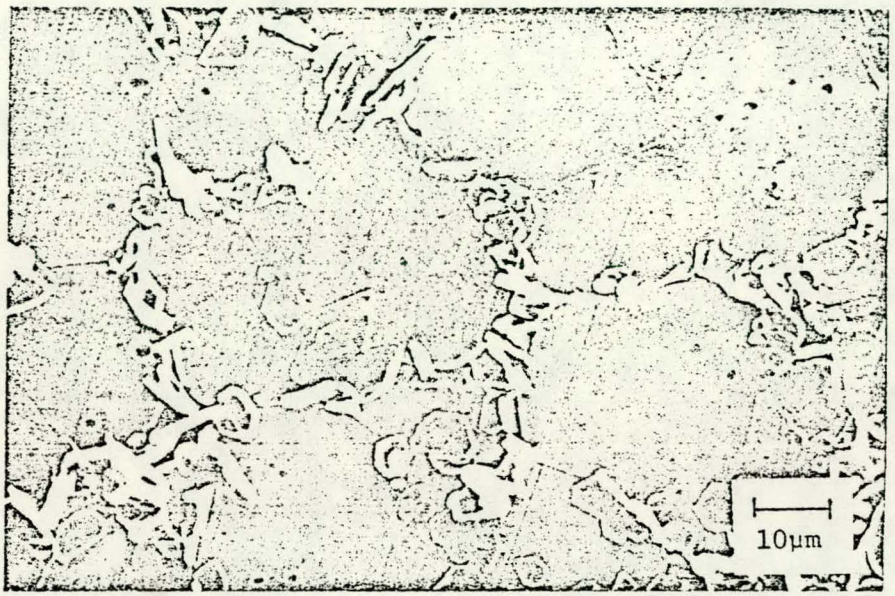

Fig 2

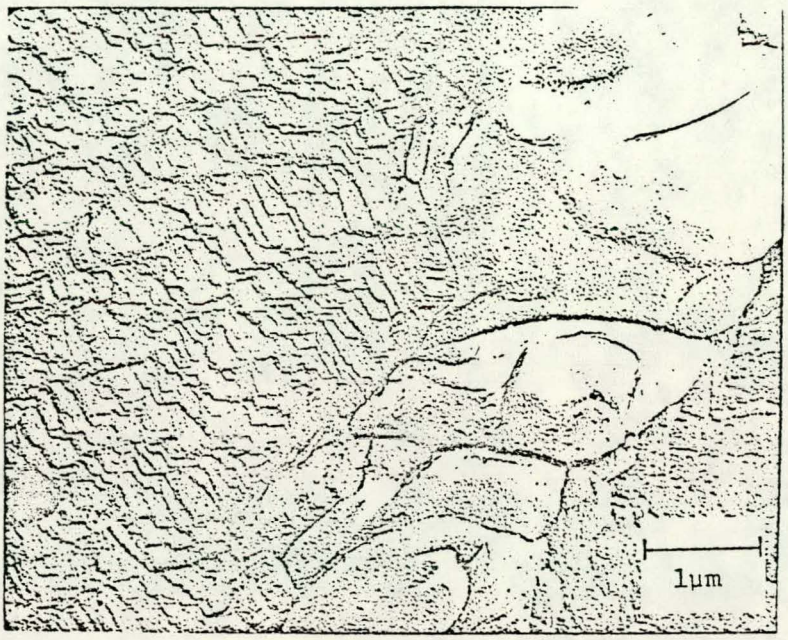

Fig 3

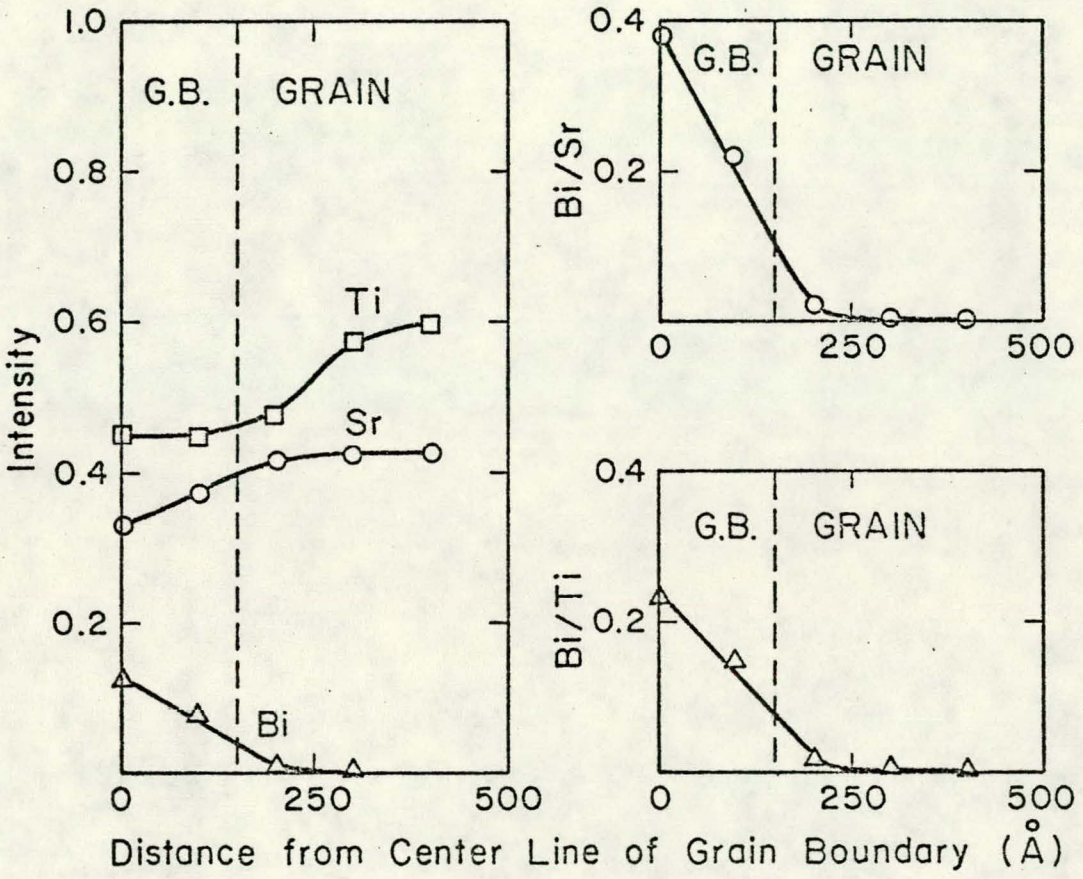
1.0
0.8
0.6
0.4
0.2
Intensity
G.B.
GRAIN
Ti
Sr
Bi
0
250
500
0.4
0.2
Bi/Sr
G.B.
GRAIN
0
250
500
0.4
0.2
Bi/Ti
G.B.
GRAIN
0
250
500
Distance from Center Line of Grain Boundary (Å)

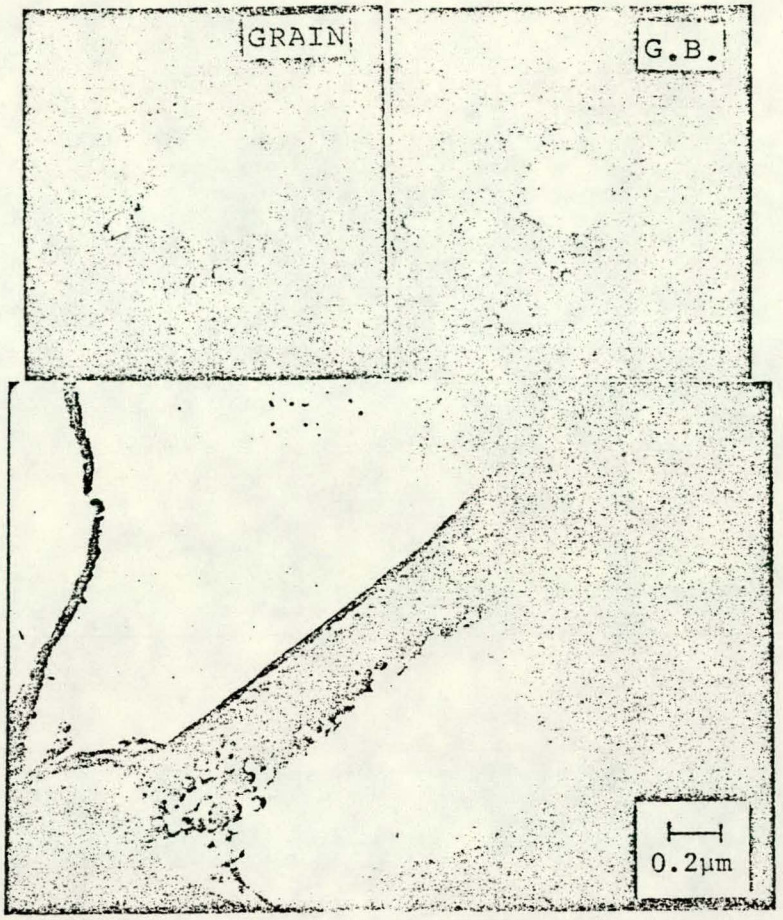
GRAIN
G.B.
0.2μm

Fig 5

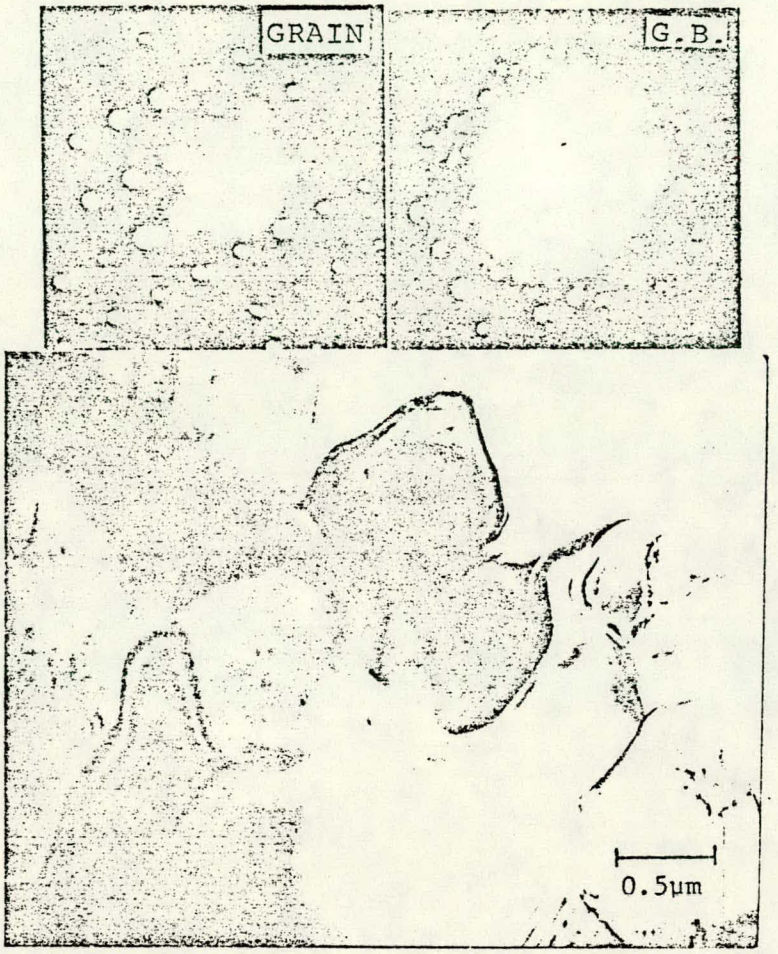

Fig 6

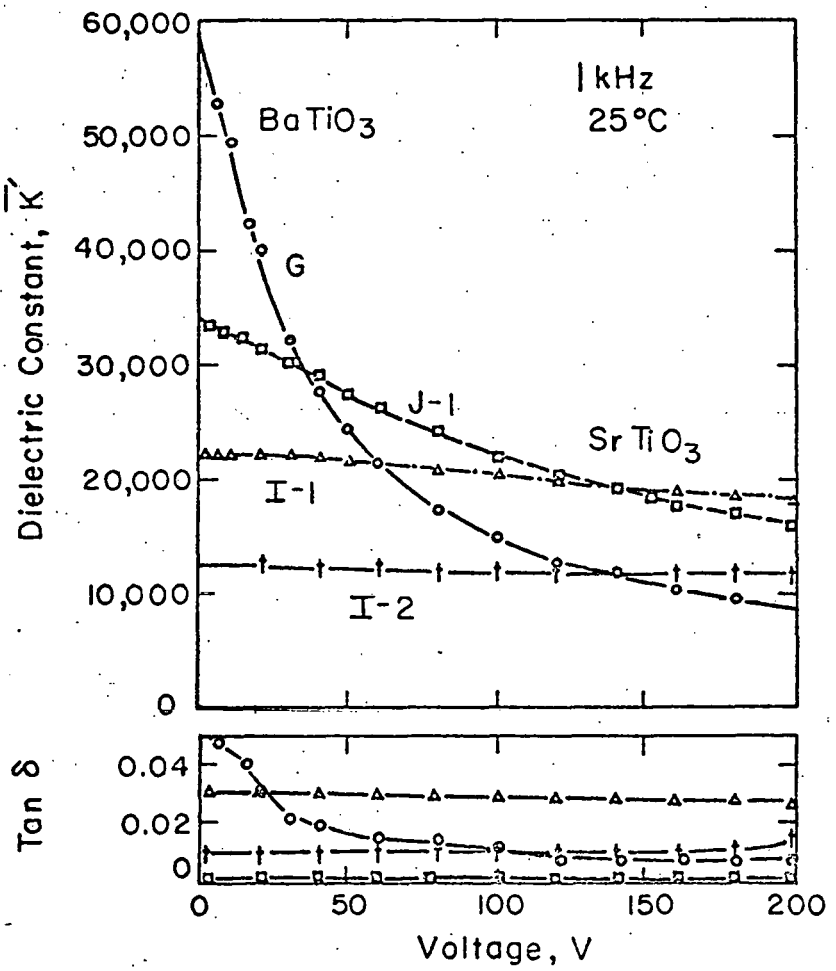
60,000
50,000
40,000
30,000
20,000
10,000
0
Dielectric Constant, K'
1 kHz
25°C
BaTiO3
G
J-1
SrTiO3
I-1
I-2
Tan δ
0.04
0.02
0
0
50
100
150
200
Voltage, V

Fig 7

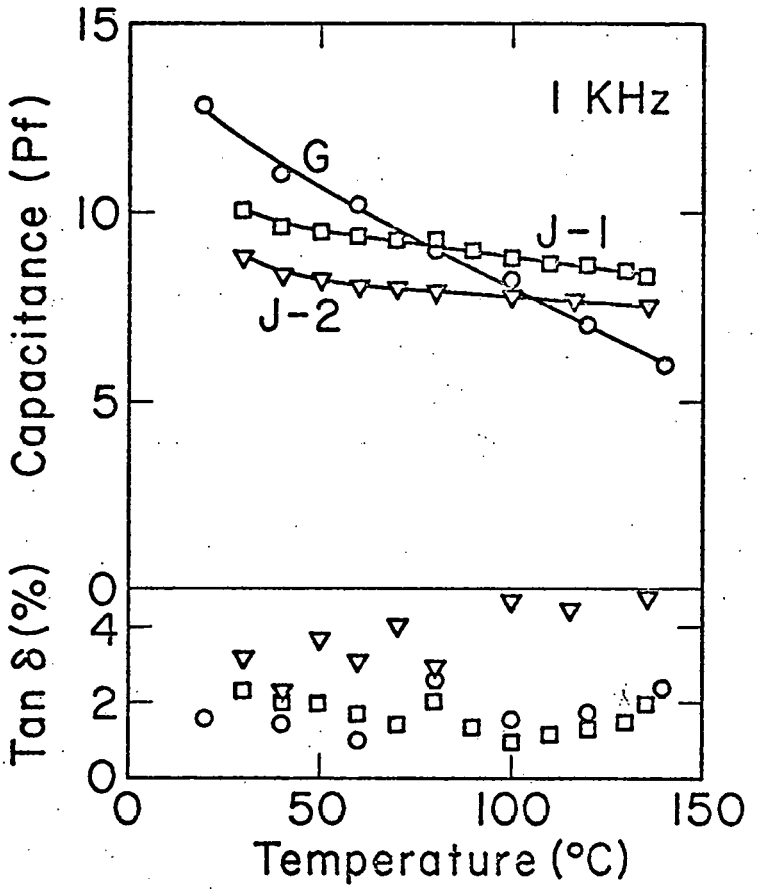
15
10
5
0
Capacitance (Pf)
1 KHz
G
J-1
J-2
4
2
0
Tan δ (%)
0
50
100
150
Temperature (°C)

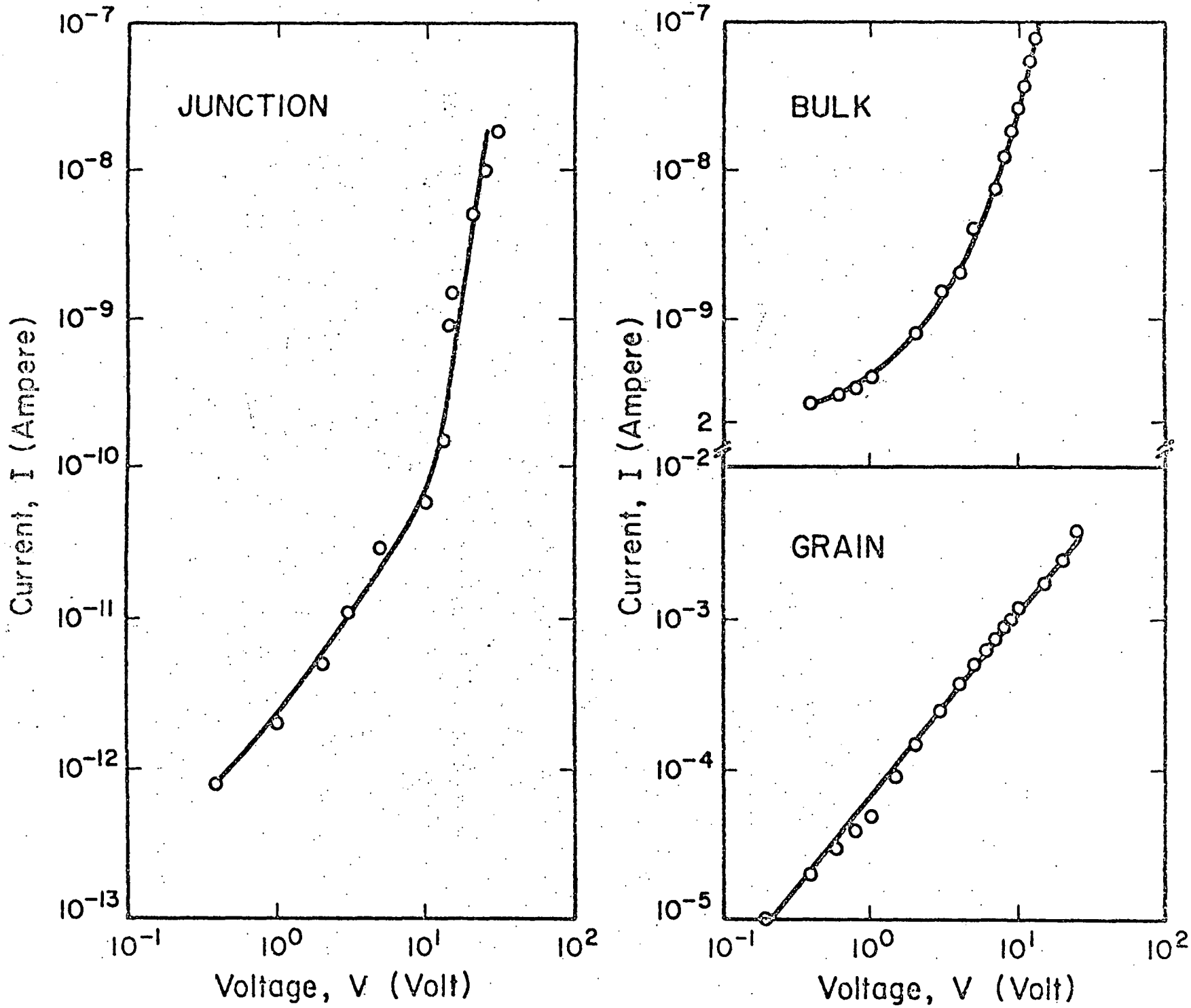
JUNCTION
BULK
GRAIN
Current, I (Ampere)
Voltage, V (Volt)
10^{-7}
10^{-8}
10^{-9}
10^{-10}
10^{-11}
10^{-12}
10^{-13}
10^{-2}
10^{-3}
10^{-4}
10^{-5}
2
10^{-1}
10^{0}
10^{1}
10^{2}

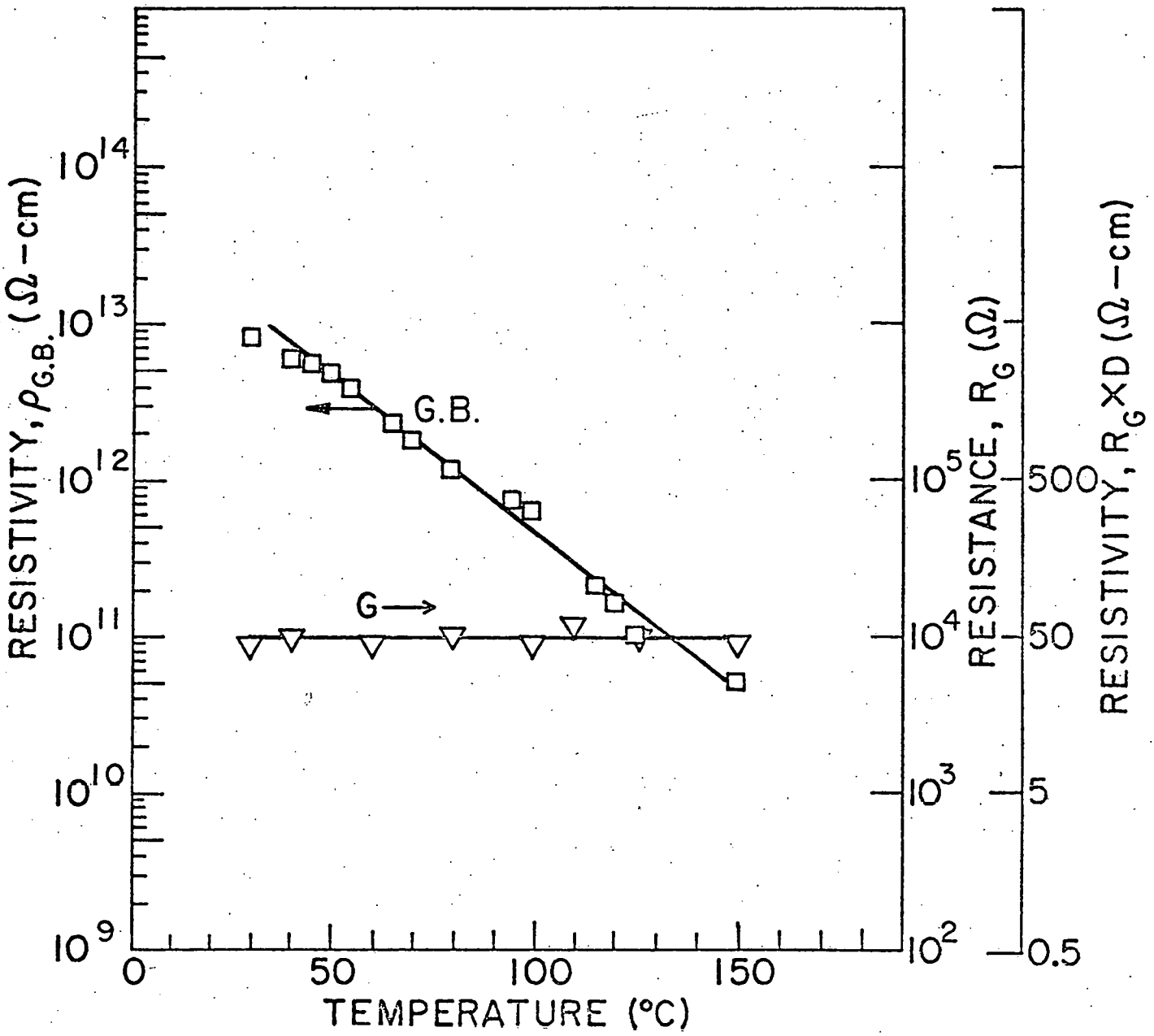
RESISTIVITY, $\rho_{G.B.}$ (Ω-cm)
10^{14}
10^{13}
10^{12}
10^{11}
10^{10}
10^{9}
G.B.
G
10^{5}
10^{4}
10^{3}
10^{2}
RESISTANCE, R_G (Ω)
500
50
5
0.5
RESISTIVITY, $R_G \times D$ (Ω-cm)
0
50
100
150
TEMPERATURE (°C)

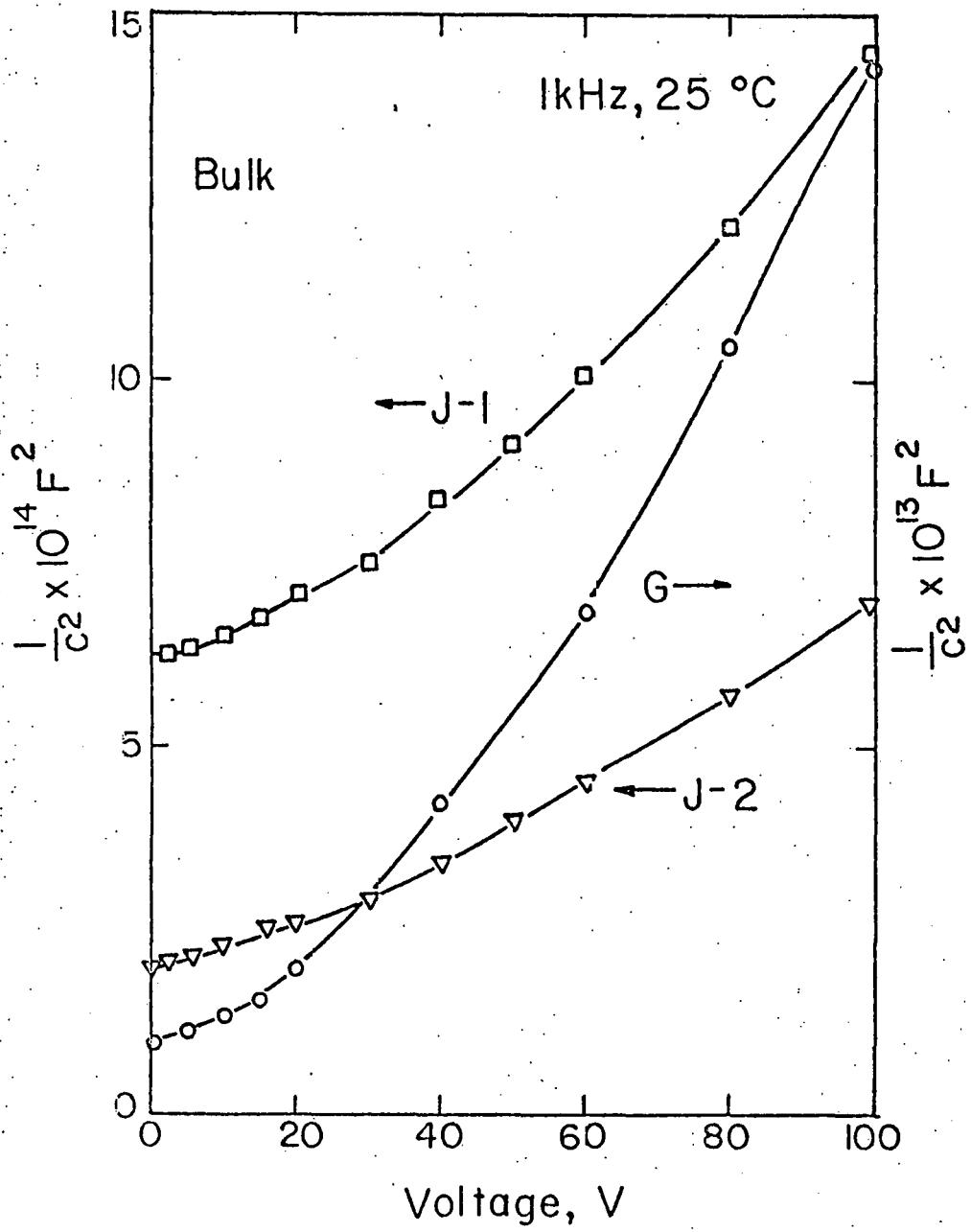
15
10
5
0
1kHz, 25 °C
Bulk
J-1
G
J-2
0
20
40
60
80
100
Voltage, V
$\frac{1}{C^2} \times 10^{14} F^2$
$\frac{1}{C^2} \times 10^{13} F^2$

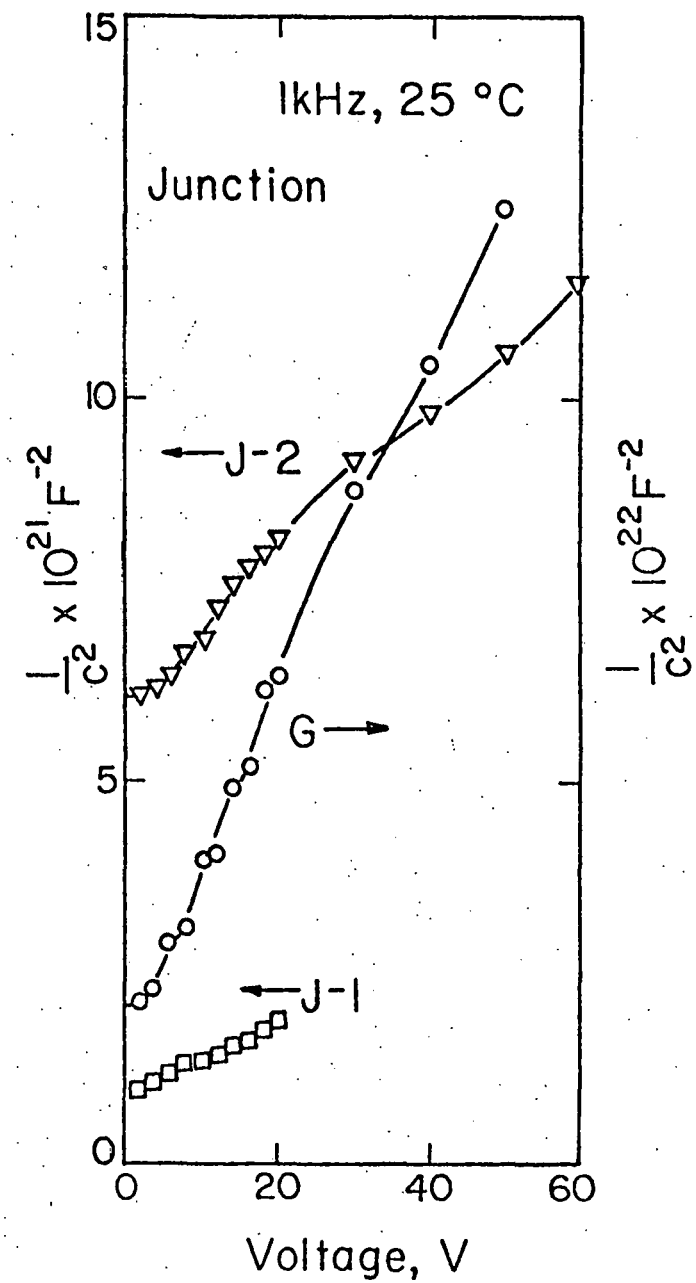
15
10
5
0
1kHz, 25 °C
Junction
J-2
G
J-1
0
20
40
60
Voltage, V
$\frac{1}{C^2} \times 10^{21} F^{-2}$
$\frac{1}{C^2} \times 10^{22} F^{-2}$

Fig 11